Biosensors and Bioelectronics 141 (2019) 111477

Contents lists available at ScienceDirect

Biosensors and Bioelectronics

journal homepage: www.elsevier.com/locate/bios

Novel thiolated-PEG linker molecule for biosensor development on gold surfaces

Han Su, Shaopei Li, Kagan Kerman*

Department of Physical and Environmental Science, University of Toronto Scarborough, 1265 Military Trial, Toronto, ON, M1C 1A4, Canada

ARTICLE INFO

Keywords:
Biosensor
Synthetic linker
PEG
Non-specific adsorption
Anti-fouling
Surface plasmon resonance
Cyclic voltammetry
Electrochemical impedance spectroscopy

ABSTRACT

The surface modifying linker molecules can directly influence the performance and longevity of biosensors. They must allow the attachment of biological recognition layer on the sensor surface, as well as the protection of the surface from fouling effects. Recent advances in this field identified several key factors that can increase the efficiency, stability and the anti-fouling effect of a layer formed by surface modifying linker molecules. Herein, this work presents a simple synthetic procedure, characterization, and application of a novel thiolated-PEG surface modifying molecule (DSPEG2) that could act as a multi-purpose linker for gold surfaces. The analyses of the molecular spatial distribution of DSPEG2 on gold surfaces were performed using time-of-flight secondary ion mass spectrometry (TOF-SIMS) imaging and X-ray photoelectric spectroscopy (XPS). The immobilization of DSPEG2 on gold surfaces was examined using cyclic voltammetry (CV), electrochemical impedance spectroscopy (EIS) and surface plasmon resonance (SPR). Our preliminary results demonstrated that DSPEG2 is a promising novel linker molecule that can be applied in a wide range of biosensors based on gold surfaces.

1. Introduction

Biosensors has been a topic of high interest for their ability to detect biomolecular interactions. At the occurrence of a biomolecular interaction at the surface of a biosensor, a physiochemical signal is detected, amplified, and transferred into quantifiable data (Fang et al., 2008). As research in this field advances to aim for better sensitivity and selectivity, the difficulty of non-specific adsorption (NSA) or fouling are increasing (Sheikh et al., 2010; Chen et al., 2017, Parrillo et al., 2017). In this article, we aimed to design and produce a novel anti-fouling linker that can be synthesized with ease and result in a stable and effective linker to immobilize biomolecules on gold surfaces.

Gold is one amongst many commonly reported substrates used for biosensor designs due to its inertness and biocompatibility. The interaction between gold and sulfur (Au–S) is a well-studied and convenient approach for the immobilization of biomolecules on gold surfaces for electrochemical and optical biosensors (Ozkan et al., 2002; Zhang et al., 2016; Veloso et al., 2014; Cheng et al., 2015). However, in the event where thiol functional groups are not present on the target subject, it may render this approach ineffective (Taheri et al., 2016). Therefore, this led to the development of a wide variety of thiol containing molecules that could serve as linkers between the gold surface and the biomolecular recognition layer. However, the orientation of the thiol-containing linker may drastically affect the performance and robustness of the sensor (Uzarski et al., 2008; Chen et al., 2014). To overcome this concern, the incorporation of aromatic substituents into the molecular design allowed π-π intermolecular interactions to stabilize the orientation of biomolecules at the event of attachment to the surface (Hunter and Sanders, 1990; Florio et al., 2005; Dou et al., 2006; Shi et al., 2016). This provides a solution that improves the overall uniformity of the layer formed by the immobilized linker.

The fouling effect of surfaces is inevitable when analyzing biological samples, that contain a variety of elements that could adhere or adsorb onto the biosensor surface non-specifically (Wiarachai et al., 2016; Wang et al., 2018, 2019). This could cause false positive results at the sensing interface, or an increase in background noise complicating the resulting data. NSA could also trigger undesired reactions that disrupt the detection process. However, due to the nature of the biosensor design, NSA could only be suppressed to a certain degree. Common anti-NSA approaches have been introduced in detail in recent publications (Wang et al., 2018, 2019). Molecules such as polyethylene glycol (PEG) and zwitterion have been tested for their anti-NSA properties Sharma et al., (2004); Otsuka et al., (2001). Although the employment of zwitterion offered excellent anti-NSA ability, its function in a flow system, as well as harsher conditions, could potentially complicate its applicability (Luk et al., 2008; Zhang et al., 2008; Cao et al.,

* Corresponding author.
E-mail address: kagan.kerman@utoronto.ca (K. Kerman).

https://doi.org/10.1016/j.bios.2019.111477
Received 17 April 2019; Received in revised form 5 June 2019; Accepted 24 June 2019
Available online 25 June 2019
0956-5663/

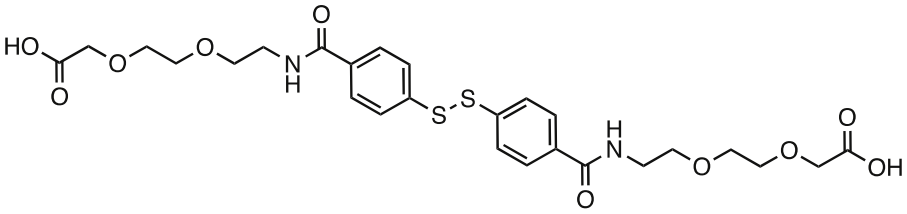

Scheme 1. Proposed structure of the thiolated-PEG linker molecule.

2014). PEG has been noted for its useful properties in anti-NSA processes becoming a widely used surface modifier in various biosensors (Prime and Whitesides, 1993; Liu et al., 2002; Bearinger et al., 2003; De Los Santos Pereira et al., 2016). Studies have shown that the presence of PEG on the sensor surface, when hydrated, provided a significant decrease in the NSA issues (Chen et al., 2010; Avci et al., 2013; Pawlowska et al., 2014; Emmenegger et al., 2009). Thus, PEG moiety was incorporated into the final molecular design of our thiolated linker molecule as shown in Scheme 1.

To connect the aromatic and PEG groups together, the two functional domains of the linker were linked together via an amide bond. Amide linkage not only provided a simple and easily achievable approach, the presence of hydrogen bond in an amide linkage could also enhance the stability and structure of the linker interface (Hermanson, 2013; Sun and Wu, 2018). Finally, incorporation of a carboxylic acid functional group at the terminal end allowed further modification to immobilize biomolecules such as proteins and antibodies via amine coupling reaction (Fischer, 2010; Li et al., 2012). Our linker molecule was synthesized via a one-pot synthesis. Upon structural characterizations, the molecule was immobilized onto a gold surface. To assess its anti-NSA properties, the modified gold surfaces were analyzed using well-established analytical techniques such as surface plasmon resonance (SPR) and electrochemistry.

2. Materials and methods

2.1. Chemicals

Spectra-grade dimethyl sulfoxide (CAS # 67-68-5), 4-mercaptobenzoic acid (CAS # 1074-36-8), ethanol (CAS # 64-17-5), methanol (CAS # 67-56-1) and dichloromethane (CAS # 75-09-2) were purchased from Sigma-Aldrich (Mississauga, ON) and used as is. High purity 1-ethyl-3-(3-dimethylaminopropyl)carbodiimide hydrochloride (CAS # 245-095-1), N, N'dicyclohexylcarbodiimide (CAS # 538-75-0)) were purchased from Thermal-Fisher Scientific (Whitby, ON) and used as is. The 2-(2-(2-Aminoethoxy)ethoxy)acetic acid (CAS # 134978-97-5) were purchased from ATK Chemical Company Limited (Shanghai, China). Methanol-d_4, 99.8% (CAS # 811-98-3) was obtained from Sigma-Aldrich (St. Louis, MO, USA).

2.2. Instruments

Column chromatography was performed on silica gel 60, 63–200 μm, obtained from Caledon Laboratory Chemicals (Georgetown, Canada). All nuclear magnetic resonance (NMR) experiments were recorded on Avance-III 500 MHz spectrometer (Bruker, Mannheim, Germany). Electron impact (EI) mass spectrometry (MS) was performed on an ABI/Sciex QStarXL mass spectrometer (Applied Biosystems, Beverly, MA).

2.3. DSPEG2 synthesis

As shown in Scheme 2, product (2) was synthesized by dissolving 4-mercaptobenzoic acid (0.1379 g, 0.894 mmol) in 5 mL DMSO. The mixture was stirred for 8 h at 70 °C. Then, 0.171 g (0.894 mmol) of 1-ethyl-3-(3-dimethylaminopropyl) carbodiimide hydrochloride was combined into the mixture and stirred for an addition 5 h in 25 °C, and N, N′-dicyclohexylcarbodiimide (0.102 g, 0.894 mmol) was added into the mixture and stirred for 8 h. To synthesize DSPEG2, 0.30 g (1.83 mmol) was combined with the previous mixture. The solution was stirred at room temperature for 24 h. Completion of the reaction was monitored by TLC. High dilution using distilled water to remove DMSO, and DSPEG2 was finally purified using 9:1 DCM: ACN with 1% acetic acid solvent system. ^{1}H NMR (500 MHz, Methanol-d_4) δ 7.80 (d, J = 7.4 Hz, 4H), 7.59 (d, J = 7.5 Hz, 4H), 4.10 (s, 4H), 3.72–3.62 (m, 12H), 3.58–3.53 (m, 4H). MS (EI) m/z 595.20 (M + 1 +).

2.4. DSPEG2 immobilization

The immobilization of DSPEG2 was performed by drop casting an aliquot (200 μL) of 2 mmol L^{-1} of DSPEG2 dissolved in Na_2CO_3 buffer (pH 8.5) onto a 1 cm × 1 cm gold wafer (100 nm Au, on silicon wafer, Western Nanofabrication Facility, London, ON) and incubated at 25 °C for 12 h. The wafers were washed and dried overnight with a gentle stream of nitrogen gas.

2.5. X-ray photoelectric spectroscopy (XPS)

Angle-resolved XPS analysis was performed with a Theta-probe Thermo-Fisher Scientific Instrument (East Grinstead, UK) with a monochromatic A1 Ka source with a photo energy 1486.6 eV. The accumulated angle was 90° with a 20 eV pass energy at the analyzer at a 10-8 mbar vacuum chamber. The analysis area was 500 μm^2.

2.6. Time-of-flight secondary ion mass-spectrometry (TOF-SIMs)

TOF-SIMs images were collected using a TOF-SIMS IV (Ion-TOF GmbH, Munster, Germany). At a 45° incident angle, the pulsed primary ion beam of focused 25 keV Ga^+ ions was used to analyze the samples. High spectral resolution images (m/Δm = 10 000) were collected using "bunch mode" with a primary ion current of 1.5 pA over a 500 × 500 μm^2 area. High spatial resolution images (ΔL = 200 nm) were also collected separately with a primary ion current of 0.8 pA over a 500 × 500 μm^2 area. Principle ion exceeded the static limit for both experiments.

2.7. Surface plasmon resonance

All SPR measurements were performed at room temperature using Biacore X100 Surface Plasmon Resonance (GE Healthcare, Life Sciences, Marlborough, MA). Biacore Sensorchip SIA Au contained 50 nm gold on glass. Both reference channel (channel 1) and measurement channel (channel 2) were conditioned with 3 consecutive injections of regeneration solution (10 mM glycine-HCl, pH 2.5) for 120 s at a flow rate of 10 μL/min. DSPEG2 Immobilization. The linker molecule DSPEG2 (1.5 μM in immobilization buffer of 100 mM Na_2CO_3, pH 10) was injected onto the channel 2 only, for 1080 s at flow rate of 5 μL/min, followed by an immobilization buffer wash for 300 s.

2.8. Anti-NSA analysis

The lyophilized human serum albumin (HSA) was dissolved in PBS

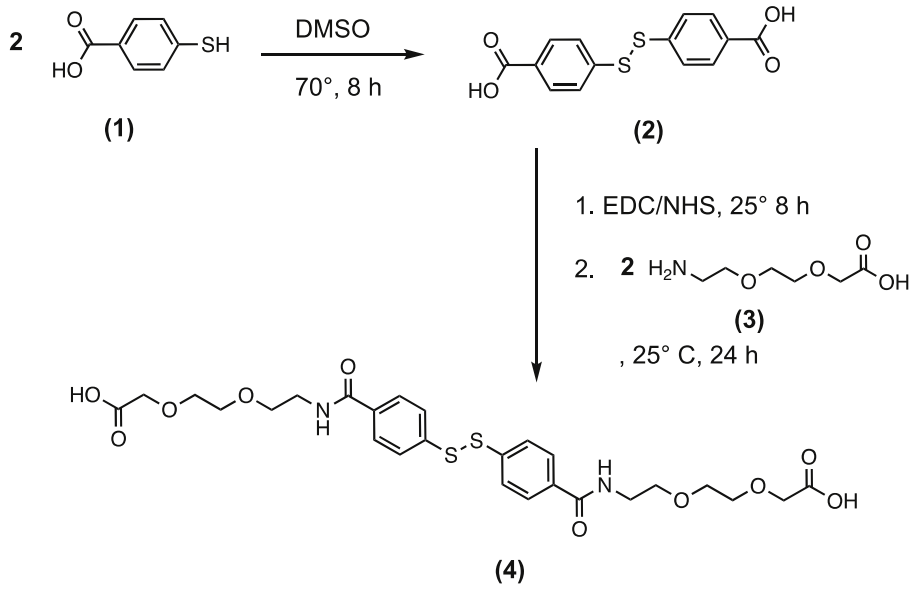

Scheme 2. Proposed reaction scheme for the synthesis of 2,2'-((((((4,4′-disulfanediylbis(benzoyl))bis(azanediyl))bis(ethane-2,1-diyl))bis(oxy))bis(ethane-2,1-diyl))bis(oxy))diacetic acid or DSPEG2.

(10 mM, pH 7.4) at desired concentrations of 3.125 mg/mL, 6.25 mg/mL, 12.5 mg/mL, 25 mg/mL and 50 mg/mL and was consecutively injected into both channels at 5 μL/min for 1080 s with 600 s PBS wash in between each injection. Adsorption of HSA was calculated from the increase in SPR response for each channel. This analysis was performed in triplicates (n = 3). All SPR experiments were analyzed using Biacore X100 Evaluation Software (GE Healthcare, Life Sciences, Marlborough, MA).

2.9. Electrochemistry

All electrochemical measurements were performed at room temperature with an Autolab PGSTAT 12 potentiostat (Metrohm Canada, ON). Cyclic voltammetry (CV) and electrochemical impedance spectroscopy (EIS) were carried out using a conventional three-electrode system with a gold electrode as working electrode, a platinum rod auxiliary electrode and an Ag/AgCl reference electrode (CH Instruments, Austin, TX). CV was performed between +0.5 V and −0.3 V with a scan rate of 0.1 V/s. EIS measurements were conducted over the frequency range of 0.1 Hz–10 kHz, using 10 mM $[Fe(CN)_6]^{3-/4-}$ or 1 mM $[Ru(NH_3)_6]^{3+}$ as the reporter molecule in 0.1 M $NaClO_4$ (pH 7.4) unless otherwise stated.

3. Results and discussion

DSPEG2 (Scheme 1) was designed with a thiol group that would allow the linker to attach onto gold surfaces. The presence of benzene would aid the layer's stability and control the orientation of the linker. PEG domains provided the desired anti-NSA properties. The carboxylate acid group towards the end of the linker was useful for further modification with biomolecules via amine coupling. The linker was prepared and synthesized according to Scheme 2. NMR (Fig. S-1) and GC-MS (Fig. S-2) were employed to support and characterize structure and purity of the products. To assess the behaviour of DSPEG2 on a gold surface, XPS and TOF-SIMS were performed.

3.1. Surface characterization

Surfaces modified with DSPEG2 were analyzed using XPS as shown in Fig. 1b with the high-resolution spectrum of Au 4f7/2. An identical signal at 84.0 eV was observed for both linker-modified and unmodified gold surfaces. Signal profiles of both spectra remained highly similar, this indicated, the modification process did not alter the nature of the gold surfaces. Secondly, in the high-resolution of the S 2p spectrum (Fig. 1a) indicated a post modification, at 163.0 eV, a significant signal increase was observed. This was expected as the presence of this signal was in connection to the Au-SR' structure formation (Xue et al., 2014), as such, was an indication that the thiol group in DSPEG2 was successfully bound to the gold surface. Fig. 1c and d shows the C 1s and O 1s peaks of the gold surfaces before and after modification with DSPEG2. On the C 1s spectrum of DSPEG2 modified the gold surface, two peaks at 286.0 eV and 289 eV related to the O–C and O–C=O structures were observed, respectively. These are commonly observed signals, when the PEG layer is presented on the surface (Popat et al., 2004) In connection, shifts of binding energy observed on O 1s spectrum supported the presence of oxygen atom species, when PEG layer was present on the gold surface. Thus, the molecular information obtained in XPS supported the successful immobilization of the linker on the gold surface.

TOF-SIMs was performed to provide a general assessment on the uniformity of the linker layer on the gold surface. Both negative and positive TOF-SIMs analyses were performed, the positive spectra will be presented in this study (Supporting information, S3), since high-quality negative TOF-SIMs spectra were challenging to obtain. Similar to previously reported work on TOF-SIMs analysis of PEG layers, characteristic signals at 55.2 and 57.3 m/z correlating to $C_3H_3O^+$ and $C_2H_3NO^+$, respectively (Cooper and Guan, 2016; Iguerb and Bertrand, 2008; Nagy et al., 2008), were found on surfaces that were immobilized with DSPEG2. Secondly, a unique peak that was found on surfaces after DSPEG2 immobilization at 332.7 m/z was attributed to be the structure $C_7H_4AuOS^+$. The corresponding TOF-SIMs images of the found ion fragments are presented in Fig. 2. During the process of TOF-SIMs imaging, an edge of the area modified with DSPEG2 was observed. The area containing $C_7H_4AuOS^+$ ions overlapped with the one generating $C_3H_3O^+$ and $C_2H_3NO^+$ ions. The layer observed on the surface was concluded to be formed by the immobilized DSPEG2. Furthermore, during the imaging process, no "signal islands" or clusters of ions were observed on the modified surfaces. This suggested that the layer formed by DSPEG2 was even, and free of large aggregates. Though further ellipsometric work is still required to study the thickness of the formed layer, our TOF-SIMS results demonstrated that the molecules detected on the modified surfaces was due to the self-assembly of DSPEG2, and

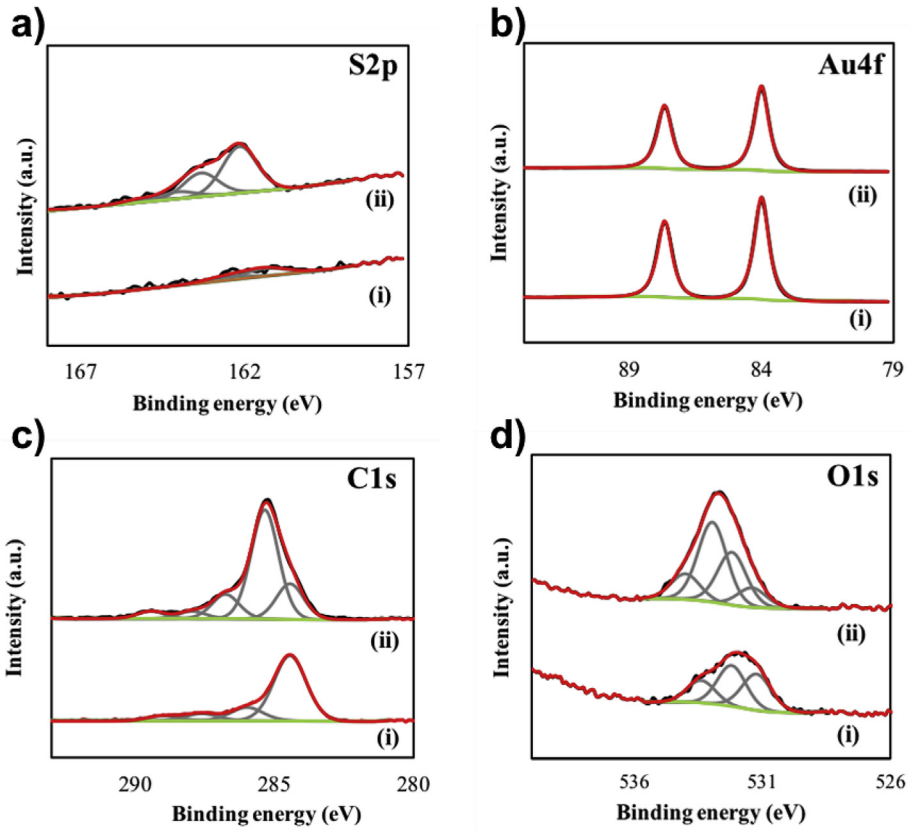

Fig. 1. XPS data plots for S2p (a), Au4f (b), C1s (c) and O1s (d) on bare gold surface (i) and DSPEG2-modified surface (ii). Modification conditions were as described in Experimental section (a.u = arbitrary units). (For interpretation of the references to colour in this figure legend, the reader is referred to the Web version of this article.)

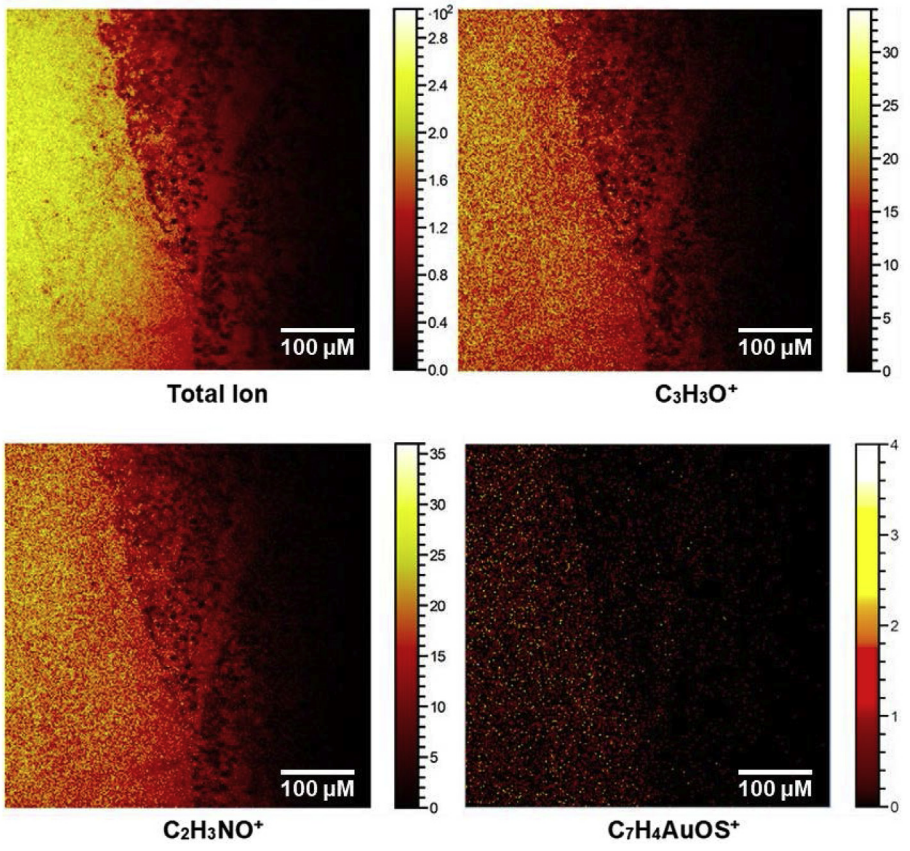

Fig. 2. Representative positive ion TOF-SIMS images showing the distribution of DSPEG2 fragments after a bare gold surface was modified with DSPEG2 as described in the Experimental section. The area of the edge, where the surface was incubated with DSPEG2 was imaged over a 500 × 500 µm^2 with the scale bar representing 100 µm. (For interpretation of the references to colour in this figure legend, the reader is referred to the Web version of this article.)

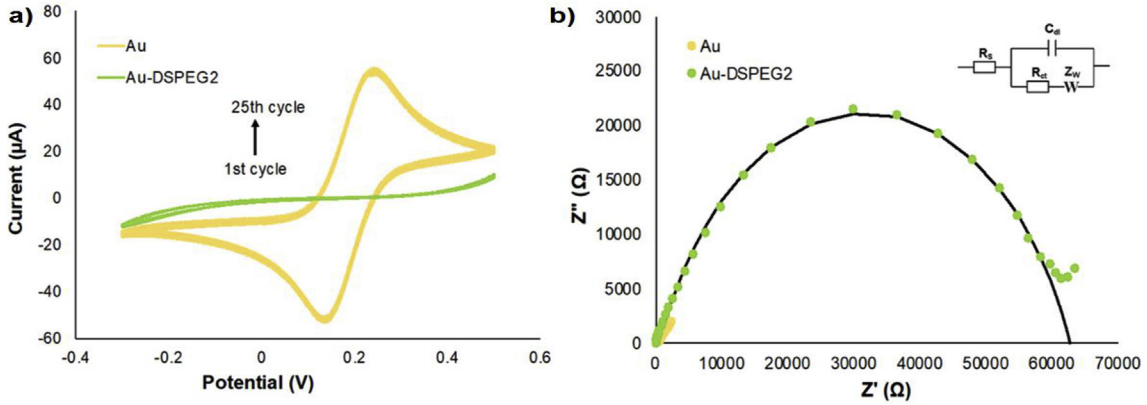

Fig. 3. a) Cyclic voltammograms at a scan rate of 0.1 V/s for 25 cycles; and b) Nyquist plots with applied frequency from 0.1 Hz to 10 kHz of bare gold electrode (yellow) and DSPEG2 modified gold electrode (green) in 10 mM $[Fe(CN)_6]^{3-/4-}$ with 0.1 M $NaClO_4$ as supporting electrolyte. The charge-transfer resistance R_{ct} values were obtained by fitting the Nyquist plot with a Randles equivalent circuit (inset). (For interpretation of the references to colour in this figure legend, the reader is referred to the Web version of this article.)

the immobilized DSPEG layers were both uniform and free of large clusters.

3.2. Electrochemical analysis

To evaluate the stability and performance of the DSPEG2 layer, cyclic voltammetry (CV) and electrochemical impedance spectroscopy (EIS) were employed (Fig. 3).

Fig. 3a demonstrated the CV analysis of DSPEG2 modified-gold surface for 25 cycles in $[Fe(CN)_6]^{3-/4-}$, compared to the unmodified gold electrode. The current flow for the modified-gold surface was negligible at the potential window of the gold electrode. This suggested that the $[Fe(CN)_6]^{3-/4-}$ molecules were unable to diffuse to the gold surface due to the presence of the linker layer (Doneux et al., 2016). CV results had also demonstrated the stability of the linker layer in multi-cycle voltammetry, as no noticeable peaks arose after multiple CV scans. As shown in Fig. 3b, the charge transfer resistance (R_{ct}) of the modified gold electrodes was approximately 62 kΩ, as predicted from the simulation of Randles equivalent circuit. In comparison to the negligible R_{ct} from the plain gold surface, the high R_{ct} from the modified gold electrode indicated that the formed linker layer on the gold surface offered a "barrier" that suppressed the diffusion of $[Fe(CN)_6]^{3-/4-}$ redox couple to the electrode surface decreasing the electron transfer at the liquid-gold interface. This could also support the successful immobilization of the linker that formed this resistive "barrier" increasing the R_{ct} (Doneux et al., 2016; Su et al., 2018).

Furthermore, the linker was also tested in a dynamic system using SPR. The analysis using SPR provided important information regarding the anti-NSA properties of DSPEG2.

3.3. SPR surface modification

First, the linker was injected onto a blank gold sensor chip. The immobilization of DSPEG2 was observed from the increase in SPR responses as demonstrated in Fig. S-3 and S-4. A kinetic affinity (K_D) of 417.5 ± 61.4 nM (n = 3) calculated using the Biacore Evaluation Software indicated a relatively strong interaction of DSPEG2 to the gold surface. The surface coverage of DSPEG2 molecules on gold surface was evaluated following a Langmuir-like isotherm (Hanaor et al., 2014):

$$\theta = \frac{\Gamma_{eq}}{\Gamma_{max}} = \frac{K\,[DSPEG2]}{1 + K\,[DSPEG2]}$$

where θ is the fractional coverage on surface and equals to 0.78. Γ_{eq} and Γ_{max} are coverage at equilibrium and saturation coverage. K is the association constant which is the inverse of K_D estimated from the SPR simulation.

3.4. Anti-NSA studies

The anti-NSA properties of DSPEG2 was also tested. HSA was exposed at various concentrations onto the modified surfaces (Zou et al., 2015; Liu et al., 2011). The resulting sensorgrams are shown in Fig. 4a. The adsorption of HSA to the modified and non-modified gold surfaces was determined by the difference of SPR responses taken before and after each HSA injection (Fig. 4a). To provide a performance comparison, two other commonly used linkers, lipoic acid (LPA) (Gu et al., 2018) and DTSSP (3,3′-dithiobis(sulfosuccinimidyl propionate)) (Veloso et al., 2014), were also tested after immobilization onto gold surfaces, followed by inactivation with 100 mM ethanolamine. The results were summarized in Table S-1. The mean values of HSA adsorption at the concentrations of 3.125 mg/mL, 6.25 mg/mL, 12.5 mg/mL, 25 mg/mL and 50 mg/mL were 83.0 RU, 121.6 RU, 124.6 RU, 133.5 RU and 193.4 RU for modified gold surface and 191.8 RU, 374.3 RU, 454.3 RU, 512.7 RU, and 681.2 RU for non-modified gold surfaces, respectively (n = 3). As the normal range of HSA concentration in serum is approximately 35–50 mg/mL (Choi et al., 2004), we utilized this range in our SPR studies. As shown in Fig. 4b, higher SPR responses were recorded for each HSA concentration on the non-modified surfaces (yellow), LPA (Red) and DTSSP (blue) modified surfaces. The NSA of HSA resulted in a concentration-dependent increase of SPR responses. On the other hand, the DSPEG2-modified surface suppressed the NSA of HSA, and the corresponding sensorgram (green) did not display any significant increase in the SPR responses. This result supported our hypothesis that DSPEG2 formed a self-assembled layer with anti-NSA properties on the gold surface.

To challenge the DSPEG2-modified surfaces, further anti-NSA tests were performed under different conditions including slightly acid (pH 5.0), slightly basic (pH 9.0), high ionic strength (500 mM NaCl), and a complex matrix (artificial cerebrospinal fluid). As shown in Fig. S-5, ΔResponse under these conditions resulted in relatively low NSA of 323 RU, 212.7 RU, 167.1 RU, and 181.5 RU, respectively. The solubility of DSPEG2 under various pH conditions were tested and the results were summarized in Table S-2. Moreover, human serum was tested on DSPEG2-modified gold surfaces to support the applicability of real samples. Due to the set-up software of the SPR instrument, up to 50% of human serum could be tested for its NSA characteristics on the DSPEG2-modified surfaces. It was observed an increase 1256 RU of NSA after continuous exposure of 3.125%, 6.25%, 12.5%, 25% and 50% of human serum in PBS, 300 RU less than of non-modified bare gold surface (Fig. S-6). As further improvements can be made based on the concept of

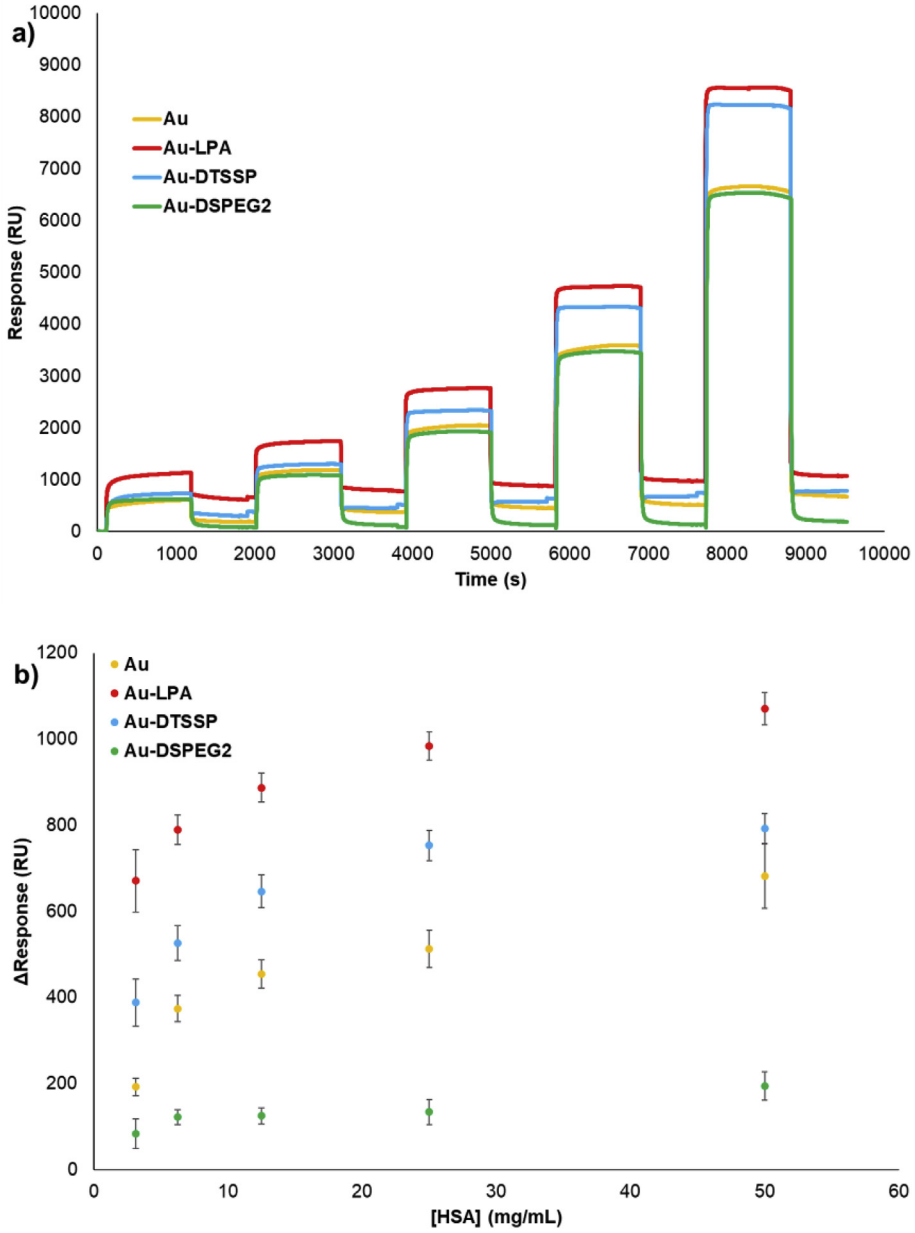

Fig. 4. SPR sensorgrams of anti-NSA measurements using various concentrations of HSA on a bare gold surface (yellow), LPA-modified gold surface (red), DTSSP-modified gold surface (blue), and DSPEG2-modified gold surface (green). a) Real time SPR responses and b) ΔResponse displays the increase in SPR response before and after the exposure to increasing concentrations of HSA. (For interpretation of the references to colour in this figure legend, the reader is referred to the Web version of this article.)

anti-NSA linkers (Sheikh et al., 2010), the synthesis of longer PEG strands is now in progress for the development of next-generation linkers in our laboratory.

4. Conclusions

In conclusion, the synthesis and characterization of the newly designed surface modifying compound DSPEG2, were demonstrated to be successful. The molecule showed high compatibility towards both static and dynamic flow system during its immobilization process. The resulting layer formed by DSPEG2 was shown to be stable and uniform. The applicability of the proposed molecule in anti-NSA analysis demonstrated a promising trend. We compared the commercially available LPA and DTSSP surface modifiers with DSPEG2 in different pH, ionic strength, and real sample matrices, and observed that DSPEG2 demonstrated a high anti-fouling effect. Thus, we envisage that these novel linker molecules with multi-functional domains would become a significant topic of interest to enhance the overall performance of biosensors.

Declaration of interests

The authors declare that they have no known competing financial interests or personal relationships that could have appeared to influence the work reported in this paper.

CRediT authorship contribution statement

Han Su: Conceptualization, Investigation, Methodology, Validation, Writing - original draft. **Shaopei Li:** Conceptualization, Investigation, Methodology, Validation, Writing - original draft. **Kagan Kerman:** Data curation, Funding acquisition, Project administration, Supervision,

Writing - review & editing.

Acknowledgments

This work was supported by the Canada Research Chair Tier-2 award to K. Kerman for “Bioelectrochemistry of Proteins” (project no. 950–231116), the Ontario Ministry of Research and Innovation (Project no. 35272), Discovery Grant (project no. 3655) from the Natural Sciences and Engineering Research Council of Canada (NSERC), and the Canada Foundation for Innovation (project no. 35272). The authors thank Dr. Todd Simpson for his technical assistance with ellipsometric measurements in the *Western Nanofabrication Facility* at Western University (London, ON). The authors also thank Dr. Rana Sodhi at the *Surface Interface Ontario* at the University of Toronto for his technical assistance with TOF-SIMS and XPS analyses.

Appendix A. Supplementary data

Supplementary data to this article can be found online at https://doi.org/10.1016/j.bios.2019.111477.

References

Avci, C., Sheikh, S., Blaszykowski, C., Thompson, M., 2013. Chem. Commun. 49, 466–468.
Bearinger, J.P., Terrettaz, S., Michel, R., Tirelli, N., Vogel, H., Textor, M., Hubbell, J.A., 2003. Nat. Mater. 2, 259–264.
Cao, B., Tang, Q., Cheng, G., 2014. J. Biomater. Sci. Polym. Ed. 25, 1502–1513.
Chen, S., Li, L., Zhao, C., Zheng, J., 2010. Polymer 51, 5283–5293.
Chen, H., Liu, F., Qi, F., Koh, K., Wang, K., 2014. Int. J. Mol. Sci. 15, 5496–5507.
Chen, P.R., Wang, T.C., Chen, S.T., Chen, H.Y., Tsai, W.B., 2017. Langmuir 33, 14657–14662.
Cheng, X.R., Wallace, G.Q., Lagugné-Labarthet, F., Kerman, K., 2015. ACS Appl. Mater. Interfaces 7, 4081–4088.
Choi, S., Choi, E.Y., Kim, D.J., Kim, J.H., Kim, T.S., Oh, S.W., 2004. Clin. Chim. Acta 339, 147–156.
Cooper, S.L., Guan, J. (Eds.), 2016. Advances In Polyurethane Biomaterials, first ed. Woodhead Publishing, USA.
De Los Santos Pereira, A., Sheikh, S., Blaszykowski, C., Pop-Georgievski, O., Fedorov, K., Thompson, M., Rodriguez-Emmenegger, C., 2016. Biomacromolecules 17, 1179–1185.
Doneux, T., De Ghellinck, A., Triffaux, E., Brouette, N., Sferrazza, M., Buess-Herman, C., 2016. J. Phys. Chem. C 120, 15915–15922.
Dou, R.F., Ma, X.C., Xi, L., Yip, H.L., Wong, K.Y., Lau, W.M., Jia, J.F., Xue, Q.K., Yang, W.S., Ma, H., Jen, A.K.Y., 2006. Langmuir 22, 3049–3056.
Emmenegger, C.R., Brynda, E., Riedel, T., Sedlakova, Z., Houska, M., Alles, A.B., 2009. Langmuir 25, 6328–6333.
Fang, C., Fan, Y., Kong, J., Gao, Z., Balasubramanian, N., 2008. Anal. Chem. 80, 9387–9394.
Fischer, M.J., 2010. Methods Mol. Biol. 627, 55–73.
Florio, G.M., Werblowsky, T.L., Müller, T., Berne, B.J., Flynn, G.W., 2005. J. Phys. Chem. B 109, 4520–4532.
Gu, X., She, Z., Ma, T., Tian, S., Kraatz, H., 2018. Biosens. Bioelectron. 102, 610–616.
Hanaor, D.A.H., Ghadiri, M., Chrzanowski, W., Gan, Y., 2014. Langmuir 30, 15143–15152.
Hermanson, G., 2013. Bioconjugate Techniques, third ed. Academic Press, USA.
Hunter, C.A., Sanders, J.K.M., 1990. J. Am. Chem. Soc. 112, 5525–5534.
Iguerb, O., Bertrand, P., 2008. Surface and Interface Analysis, vol 40. Wiley-Blackwell, Germany, pp. 386–390.
Li, N., Brahmendra, A., Veloso, A.J., Prashar, A., Cheng, X.R., Hung, V.W.S., Guyard, C., Terebiznik, M., Kerman, K., 2012. Anal. Chem. 84, 3485–3488.
Liu, J.T., Chen, C.J., Ikoma, T., Yoshioka, T., Cross, J.S., Chang, S.J., Tsai, J.Z., Tanaka, J., 2011. Anal. Chim. Acta 703, 80–86.
Liu, V.A., Jastromb, W.E., Bhatia, S.N., 2002. J. Biomed. Mater. Res. 60, 126–134.
Luk, V.N., Mo, G.C., Wheeler, A.R., 2008. Langmuir 24, 6382–6389.
Nagy, G., Lu, P., Walker, A.V., 2008. J. Am. Soc. Mass Spectrom. 19, 33–45.
Otsuka, H., Nagasaki, Y., Kataoka, K., 2001. Mater. Today 4, 30–36.
Ozkan, D., Erdem, A., Kara, P., Kerman, K., Gooding, J.J., Nielsen, P.E., Ozsoz, M., 2002. Electrochem. Commun. 4, 796–802.
Parrillo, V., de los Santos Pereira, A., Riedel, T., Rodriguez-Emmenegger, C., 2017. Anal. Chim. Acta 971, 78–87.
Pawlowska, N.M., Fritzsche, H., Blaszykowski, C., Sheikh, S., Vezvaie, M., Thompson, M., 2014. Langmuir 30, 1199–1203.
Popat, K.C., Sharma, S., Desai, T.A., 2004. J. Phys. Chem. B 108, 5185–5188.
Prime, K.L., Whitesides, G.M., 1993. J. Am. Chem. Soc. 115, 10714–10721.
Sharma, S., Johnson, R.W., Desai, T.A., 2004. Biosens. Bioelectron. 20, 227–239.
Sheikh, S., Sheng, J.C.C., Blaszykowski, C., Thompson, M., 2010. Chem. Sci. 1, 271–275.
Shi, D., Shen, J., Zhao, Z., Shi, C., Chen, M., 2016. Polymers 8, 92.
Su, H., Li, S., Terebiznik, M., Guyard, C., Kerman, K., Su, H., Li, S., Terebiznik, M., Guyard, C., Kerman, K., 2018. Sensors 18, 2668.
Sun, W., Wu, P., 2018. Phys. Chem. Chem. Phys. 20, 20849–20855.
Taheri, R.A., Rezayan, A.H., Rahimi, F., Mohammadnejad, J., Kamali, M., 2016. Biointerphases 11, 041006.
Uzarski, J.R., Tannous, A., Morris, J.R., Mello, C.M., 2008. Colloids Surfaces B Biointerfaces 67, 157–165.
Veloso, A.J., Chow, A.M., Ganesh, H.V.S., Li, N., Dhar, D., Wu, D.C.H., Mikhaylichenko, S., Brown, I.R., Kerman, K., 2014. Anal. Chem. 86, 4901–4909.
Wang, G., Su, X., Xu, Q., Xu, G., Lin, J., Luo, X., 2018. Biosens. Bioelectron. 101, 129–134.
Wang, Y.-S., Yau, S., Chau, L.-K., Mohamed, A., Huang, C.-J., 2019. Langmuir 35, 1652–1661.
Wiarachai, O., Vilaivan, T., Iwasaki, Y., Hoven, V.P., 2016. Langmuir 32, 1184–1194.
Xue, Y., Li, X., Li, H., Zhang, W., 2014. Nat. Commun. 5, 4348.
Zhang, H., She, Z., Su, H., Kerman, K., Kraatz, H.-B., 2016. Analyst 141, 6080–6086.
Zhang, Z., Chao, T., Jiang, S., 2008. J. Phys. Chem. B 112, 5327–5332.
Zou, Q., Kegel, L.L., Booksh, K.S., 2015. Anal. Chem. 87, 2488–2494.